ARTICLE

WILEY▪VCH

Simulation of wire metal transfer in the cold metal transfer (CMT) variant of gas metal arc welding using the smoothed particle hydrodynamics (SPH) approach

Simulation des Metalldrahttransfers bei der Kaltmetalltransfer-Variante (CMT) des Metallschutzgasschweißens unter Verwendung des geglätteten Partikel-basierten hydrodynamischen (SPH) Ansatzes

O. Mokrov[1] | S. Warkentin[1] (iD) | L. Westhofen[2] (iD) | S. Jeske[2] | J. Bender[2] | R. Sharma[1] (iD) | U. Reisgen[1] (iD)

[1]RWTH Aachen University, Welding and Joining Institute, Aachen, Germany

[2]RWTH Aachen University, Visual Computing Institute – Computer Animation, Aachen, Germany

Correspondence
S. Warkentin, RWTH Aachen University, Welding and Joining Institute, 52062, Aachen, Germany.
Email:
sergej.warkentin@isf.rwth-aachen.de

Abstract

Cold metal transfer (CMT) is a variant of gas metal arc welding (GMAW) in which the molten metal of the wire is transferred to the weld pool mainly in the short-circuit phase. A special feature here is that the wire is retracted during this strongly controlled welding process. This allows precise and spatter-free formation of the weld seams with lower energy input. To simulate this process, a model based on the particle-based smoothed particle hydrodynamics (SPH) method is developed. This method provides a native solution for the mass and heat transfer. A simplified surrogate model was implemented as an arc heat source for welding simulation. This welding simulation model based on smoothed particle hydrodynamics method was augmented with surface effects, the Joule heating of the wire, and the effect of the electromagnetic forces. The model of metal transfer in the cold metal transfer process shows good qualitative agreement with real experiments.

KEYWORDS
cold metal transfer (CMT), free surface deformation, gas metal arc welding (GMAW), simulation, smoothed particle hydrodynamics (SPH)

Abstract

Kaltmetalltransfer-Schweißen (CMT) ist eine Variante des Metallschutzgas-schweißens, bei welchem das geschmolzene Metall des Drahtes hauptsächlich

in der Kurzschlussphase in das Schmelzbad übertragen wird. Eine Besonderheit dabei ist, dass bei diesem stark gesteuerten Schweißprozess der Draht zurückgezogen wird. Dies erlaubt eine kontrollierte, spritzerfreie Ausbildung der Schweißnähte mit geringerem Energieeintrag. Um diesen Prozess zu simulieren, wird ein Modell auf Basis der geglätteten partikelbasierten hydrodynamischen (SPH) Methode entwickelt. Für die Masse- und Wärmeübertragung stellt die geglättete partikelbasierte hydrodynamischen Methode native Lösungen dar. Ein vereinfachtes Ersatzmodell wurde als Lichtbogenwärmequelle implementiert. Die Oberflächeneffekte, die Joule-Erwärmung des Drahtes und die Wirkung der elektromagnetischen Kräfte schließen den Kreis der physikalischen Phänomene der Simulation ab. Das Model der Metallübertragung bei dem Kaltmetalltransferprozess zeigt eine gute qualitative Übereinstimmung mit realen Versuchen.

1 | INTRODUCTION

Industrial production has seen numerous shifts and changes since the onset of the industrial age, with each development introducing a new strategy or technique that has significantly altered manufacturing procedures. One such development is the emergence of complex regulation techniques of the gas metal arc welding (GMAW) process, including mechanical and electrical parameters [1]. A successful variation of digital control of the gas metal arc welding process is the so-called cold metal transfer (CMT). As an emerging technology originating in industry in the early 21st century, this technique brought a new dimension to welding practices, addressing a range of limitations commonly associated with traditional methods [2]. This technique is an advanced bi-directional wire control (BDWC) process with a mechanically assisted droplet transfer [1].

The concept of cold metal transfer is characterized by its unique wire movement; in contrast to conventional welding methods, the wire in cold metal transfer recoils during the short-circuit stage, a feature that helps to prevent spatter formation and categorizes it as a low heat input process. Compared to the superordinated gas metal arc welding process its characteristic can be particularly beneficial when dealing with thin sheets and dissimilar metals, which have previously proven challenging for traditional welding methods. Further, the lower heat input minimizes distortion and thermal stresses, contributing to welds of a high standard [2, 3].

This study aims to scrutinize the physical occurrences during the bi-directional wire control welding technique, the formulation of these processes, the challenges encountered during this modeling, and the recent computational modeling frameworks utilized in these simulations. It should be emphasized that the present work is limited to the consideration of the bi-directional wire control process, which concentrates on the regulation of mechanical and electrical parameters in the short-circuit phase [1].

The central objective of this work is the creation of a model for this controlled welding variant specific mass transfer using smoothed particle hydrodynamics (SPH), considering the influencing factors of the corresponding physical phenomena.

The renowned and established finite element method (FEM) is deliberately bypassed in the present concept. The finite element method approach reliably provides insights into profound physical effects, which are not in the foreground for an industrial application and thus do not need to be captured in the high accuracy typical for a finite element method calculation. Therefore, the compensation models and surrogate models are relied upon in combination with the Lagrangian smoothed particle hydrodynamics method to produce results faster and with reduced computational demand.

2 | STATE OF THE ART

The bi-directional wire control welding technique uses a sequence of detailed physical processes that are distinct from traditional welding methods. Regulated by inverter

power sources, this process manages the welding current and voltage, along with wire speed and movement direction, Figure 1. The welding wire, upon contacting the base material, initiates a short-circuit. The welding current then decreases. Afterward, the wire recoils, terminating the short-circuit and reigniting the arc. This repeated process results in a lower average temperature and heat input compared to traditional welding methods, possibly improving the weld quality and broadening the potential material choices [4].

The bi-directional wire control technique has two characteristic modes: the arc phase and the short circuit phase. The sequence pictures 1, 4, 5 and 6 depict the arc phase with a high energy input and a wire direction towards the melt pool, Figure 1. During this phase the wire tip, poled as anode, and the base material, cathode, are heated by the processes in the electrode layers. When the material of the electrodes is in contact, the short circuit phase sets in, sequence pictures 2 and 3, Figure 1. The energy input in this phase is reduced to a minimum, on the one hand to ensure the liquid state of the contact region. On the other hand, the electrical current induces the Ampère' effect that is the main force for the occurring metal transfer. A simultaneous wire retraction promotes droplet detachment and thus enhances metal transfer. It should be emphasized that the metal transfer only takes place during the short-circuit phase. These physical occurrences, resulting among others from combinations of welding parameters, are pivotal in determining the quality of the weld. For instance, variables such as the wire feed velocity, welding speed, and current - all of which can be tailored according to the specific material and thickness combination - can significantly alter the
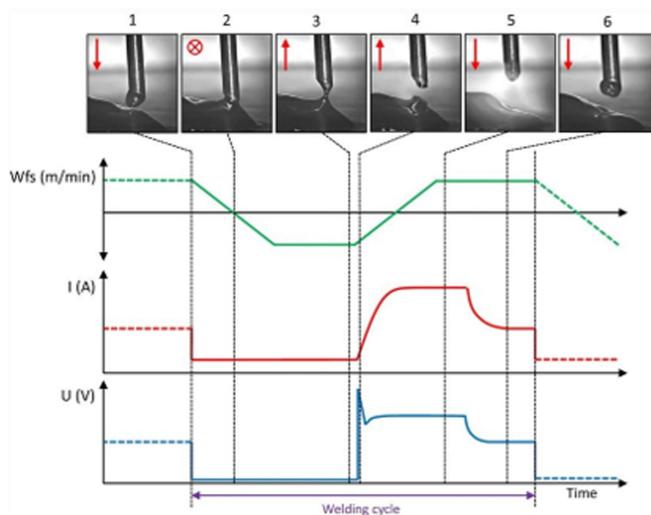
weld bead shape, the heat-affected zone (HAZ), and the mechanical attributes of the weld.

The complex physical phenomena at play in the bi-directional wire control welding make understanding and conceptualizing these processes a significant challenge. Throughout the years, numerous models have been proposed with the aim of simulating the gas metal arc welding with dynamic feeding. These models can be broadly categorized pursuing two main goals: structure simulation and process simulation. While the structure simulation aims at determining stress states as well as distortion, the process simulation investigates the processes of heat input as well as arc connection.

An established standard technique in structure simulation for the consideration of the heat input by the arc is the usage of an equivalent heat source at the cathode [5]. The heating of the anode in these cases is mimicked by the introduction of liquid droplets without the consideration of the whole physical process of melting and droplet detachment [5]. A disadvantage of this method is an unrealistic temperature distribution. In addition, this approach results in non-self-consistent models where the heat source and current source are not connected. This creates the need to recalibrate the model for each parameter change.

On the other hand, a detailed consideration of physical phenomena in process simulation delivers a deeper insight in the heat transfer, fluid flow, and solidification during the welding process, providing a comprehensive understanding of the procedure [6]. A significant challenge of this approach is the computational cost. High-fidelity models using the finite element method (FEM) or the finite volume method (FVM) that can accurately portray the bi-directional wire control technique often demand substantial computational resources. This high computational demand constrains the models' applicability for real-time control and optimization of the welding procedure.

While considerable progress has been made in modeling of dynamic feeding welding variant, various challenges remain. A primary hurdle is accurately representing the dynamic characteristics of the bi-directional wire control technique. The reciprocating wire movement and periodic short-circuits, essential features of the dynamic feeding welding method, make it difficult to model the transient heat transfer and metal transfer accurately. The movement of the wire, if taken into account, is typically preset by a frequency according to measured frequencies in experiments [6]. In contrast, the model presented in this work has an open interface and can incorporate real control data as input parameters.

Additionally, the multiscale aspect of the welding process adds another layer of complexity. The bi-

FIGURE 1 A typical sequence in a bi-directional wire control process: highly regulated course of the current, voltage and wire feed speed [4].

directional wire control technique involves a multitude of phenomena occurring on different scales - from microscale phenomena at the arc and droplet level to macroscale heat transfer and solidification. This necessitates the creation of models that can accurately depict these processes at varying time and space scales. A widely used technique for resolving the free surface of the weld pool or the droplet form is the level set method [6]. Its drawback is the need of a high-resolution grid in phase change areas.

The described challenges define requirements to the modelling process which cannot be met with the established mesh-based methods and thus cannot be applicable for real-time control and optimization of the welding procedure.

Smoothed particle hydrodynamics (SPH), a relatively nascent method in the realm of welding simulations, brings advantages on this field regarding the calculation time, in solving fluid flow and mass transfer problems and especially in the resolution of phase change interfaces. This mesh-free method is particularly suitable for modeling large deformations and free surfaces, such as the molten pool and droplet formation. Smoothed particle hydrodynamics operates by representing fluid as an aggregation of particles, with physical quantities calculated based on the characteristics of these particles. Designed for astrological calculations it was adopted to fluid flow simulation [7–10]. This approach offers an innovative perspective for understanding and predicting the welding procedure. This method has already been successfully used for different welding processes [11–13].

However, to the best of the authors' knowledge, there are no reported studies on the application of smoothed particle hydrodynamics for any variant of digitally controlled gas metal arc welding simulations. Given the potential advantages that smoothed particle hydrodynamics can offer, such as its ability to handle large deformations and free surfaces, it presents a promising avenue for future research [14,15]. The exploration and development of smoothed particle hydrodynamics for bi-directional wire control techniques simulations could provide insights that further enhance the comprehension of this exceptional technology and its applications.

3 | MODEL DESCRIPTION

To model the bi-directional wire control process, it is necessary to detect the two characteristic phases because they define which physical processes must be considered subsequently. This is done by a clustering algorithm that detects two different parts in the arc phase and only one contiguous part in the short-circuit phase.

When the actual process phase is determined following assumptions and models are applied:

Arc phase, Figure 2:

- arc heating of the anode and cathode
- resistive heating in wire
- wire feed to the melt pool with a velocity maximum according to the wire feed rate and a non-uniform movement at the turning points
- electromagnetic forces are neglected in this phase

The electromagnetic forces are neglected in this phase because no droplet separation takes place at the anode in the real process and therefore no computing power should be used to determine a quantity that does not have a high impact on the overall process. The main task of the surrogate model in the arc phase is the heating of the anode and cathode. This is the main focus. In the cathode region, consisting of the liquid molten pool and the forming weld, the influence of the electromagnetic forces on the liquid flows and thus also on the shape of the weld is of high importance. Currently, however, no method for simulating the electromagnetic fields using smoothed particle hydrodynamics (SPH) is available, since every physical quantity in smoothed particle hydrodynamics (SPH) requires a carrier mass and the area of the arc is currently a mass-free space. It is planned to integrate the effect of electromagnetism as external forces resulting from Euler calculations for stationary geometry configurations as boundary conditions in the smoothed particle hydrodynamics (SPH) model.
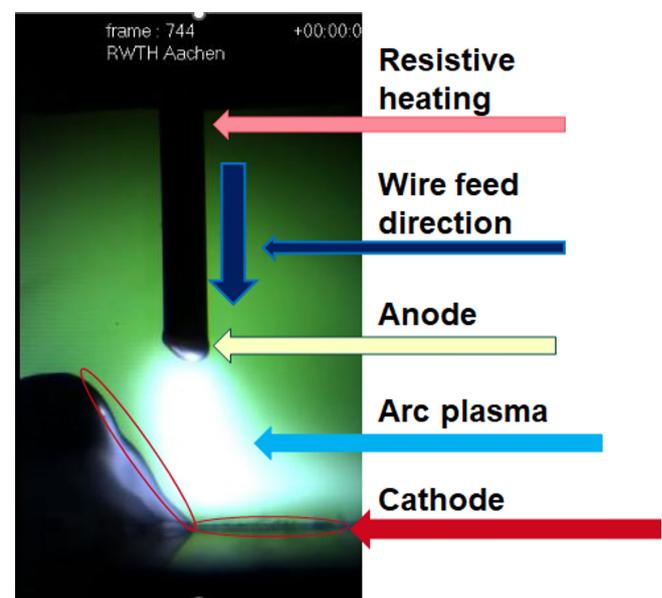

FIGURE 2 Arc phase in the bi-directional wire control process, considered physical phenomena.

Short-circuit phase, Figure 3:

– resistive heating in wire and droplet detachment area
– consideration of the Lorentz force
– wire retraction with a non-uniform movement at the turning points
– no arc heating

The simulation model is implemented in Python. A C/C++ based open-source framework named SPlisHSPlasH is used to solve the governing equations. SPlisHSPlasH can be operated via a graphical user interface (GUI) or Python. This framework is capable to solve fluid flow and heat transfer problems and also includes methods for viscosity and surface tension consideration.

The computational method adopts the fluid flow governing Navier-Stokes equations and the heat transfer governing Fourier equation to the smoothed particle hydrodynamics formalism. In smoothed particle hydrodynamics the fluid is divided into many small particles that can move relative to each other depending on their position and the surrounding particles. The particles are sample points of the underlying fluid mass and the fluid properties are represented by the particle properties. The determination of a quantity $A(x_i)$ at the position x_i is approximated using following summation over the neighboring particles j:

$$A(x_i) = \Sigma_{j \in N_{x_i}} \frac{m_j}{\rho_j} A(x_j) W(x_i - x_j; h_{smooth}) \tag{1}$$

m_j is the mass and ρ_j is the density of a particle at the position x_j. Here $W(x_i - x_j; h_{smooth})$ denotes the kernel function with smoothing length h_{smooth} and N_{x_i} denotes the set of particles within the compact support radius around x_i. Since the kernel function is a continuously
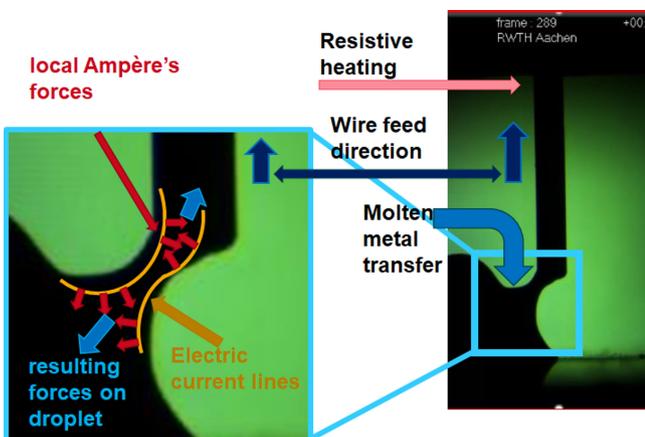
differentiable function and additionally fulfills a set of other properties this approximation can be used for the calculation of differential operators:

$$\nabla_i A(x_i) = \Sigma_{j \in N_{x_i}} \frac{m_j}{\rho_j} A(x_j) \nabla_i W(x_i - x_j; h_{smooth}) \tag{2}$$

Thus, the derivative of a quantity is formed by the derivative of the kernel function [7, 8]. The presented model is built upon the bases developed for TIG welding and droplet impact in thermal spraying [11, 14].

3.1 | Surrogate model for the arc heating effect

The concept describes the heat input into the anode and cathode. The arc is assumed to be axisymmetric. Phenomenological processes in the arc and in the layers can be based on the models of Simon and Semenov [16, 17]. The consequence of these models is that the heat input happens in layers by recombination. These models are necessary for the quantitative agreement of the overall process model. However, they require consideration of both the layer processes and the simulation of arc plasma. Since the present work aims to demonstrate the mass transfer in the short-circuit phase with the smoothed particle hydrodynamics method, it is not intended to cover the arc phase to such high accuracy. Thus, instead of these correlations, a strongly simplified surrogate model will be used. As a simplification, the global heat input is plotted for both the cathode and the anode using the same concept:

$$q'' = |j| \frac{wf}{e} \tag{3}$$

where q'' is the surface heat input, j is the electric current density, wf is the work function, e is the electron charge. It is assumed that the electric current density is evenly distributed within the layers, Figure 4. Based on the ideas from the work of Semenov and Simon, an effective current density is derived, which can be used to determine the effective areas of the cathode and anode regions [16, 17]. The distribution in the fictitious cathode and anode regions are projected onto real edge particles in the region of the droplet (anode) and the molten bath (cathode). This results in a conformal mapping to the edge particles.

The next computational task is to convert the surface heat density into a volumetric heat source distributed among the particles in the boundary layer. For this purpose, a smoothed particle hydrodynamics specific, so-

FIGURE 3 Short-circuit phase in bi-directional wire control process, considered physical phenomena.

called color function cf is used. This function delivers values between 1 and 0, which characterize the filling of an imaginary volume within the support radius with particles. A value of 1 means that a particle with the corresponding support radius is located in a fully dense region. The closer the particles are to the surface, the lower the values of the color function are. This is because the imaginary volume inside the support radius contains less particles in sum when moving out of the material. Numerically this concept uses the gradient of the color function resulting in the detection of the maximum gradient magnitude for the determination of the surface line.

This rough simplification is compensated with weighting factors using the smoothed particle hydrodynamics formalism. The weighting is taking into account the distance of the particles to a reference point, factor $F_{i,D}$, the orientation of the corresponding surface normal in relation to the wire feed direction, factor $F_{i,O}$, a factor for the exclusion of interior particles, $F_{i,S}$ and at least a limitation factor for a maximal particle temperature, $F_{i,T}$. A particle in the calculation domain obtains an energy increment according to the following equation:

$$Q_i = q'' \cdot \nabla cf \cdot V_i \cdot F_{i,D} \cdot F_{i,O} \cdot F_{i,S} \cdot F_{i,T} \qquad (4)$$

where $F_{i,D}$ is a kernel based approximation of a Gaussian distribution accounting for the distance from the reference point (representing the solid wire tip) to the evaluated point on the workpiece, Figure 4. It is calculated as following:

$$F_{i,D} = \sigma \begin{cases} 1 - 6q^2 + 6q^3, & 0 < q \le 0.5 \\ 2(1-q)^3, & 0.5 < q \le 1 \\ 0, & otherwise \end{cases} \qquad (5)$$

$F_{i,\,D}$ is a cubic distance factor with:

$$q = \frac{\|x_i - x_j\|}{h_{smooth}} \qquad (6)$$

$F_{i,O}$ establishes a main arc direction by the following scalar product:

$$F_{i,O} = \vec{r}_{N,feed} \cdot \vec{r}_{N,surface} \qquad (7)$$

For example, particles located on the perimeter of the wire have the biggest angle difference between their normal and the wire feed direction, thus the energy input on the wire perimeter is very low, Figure 4.

By the application of the factor $F_{i,S}$, the heat is added to the outer layers of particles, that discretize the computational domain, and propagates by conduction into the interior. The selection of the surface particles is made by the coverage normal [9]. The normal vector $\hat{n}_i$ shows in the direction of the lowest particle density in the particle neighborhood, Figure 5. Particle i is classified as a surface particle if there is no other particle j in the direction of $\hat{n}_i$ in a cone with an angle of $\varphi = 35°$ [11]. The energy input into the particles lying inside is thus eliminated as follows:

$$F_{i,S} = \begin{cases} 1, & \varphi = 35° < cos^{-1}\left(\hat{n}_i \cdot \frac{(x_j - x_i)}{\|x_j - x_i\|}\right) \\ 0, & otherwise \end{cases} \qquad (8)$$

A limitation factor $F_{i,T}$ controls the heat input by accounting for the evaporation temperature of the material T_V. It is calculated as:
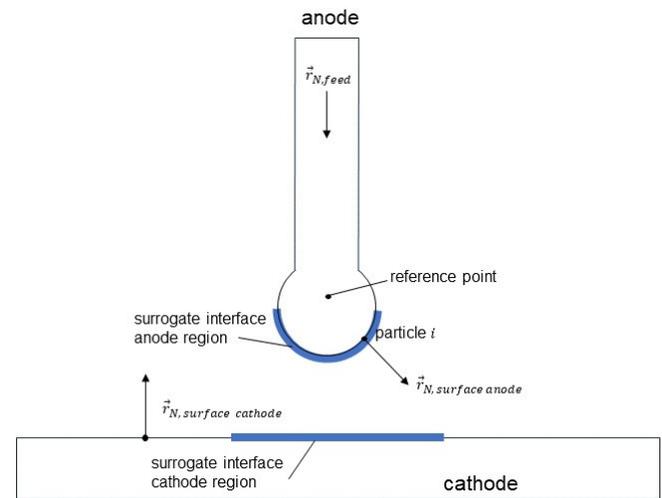

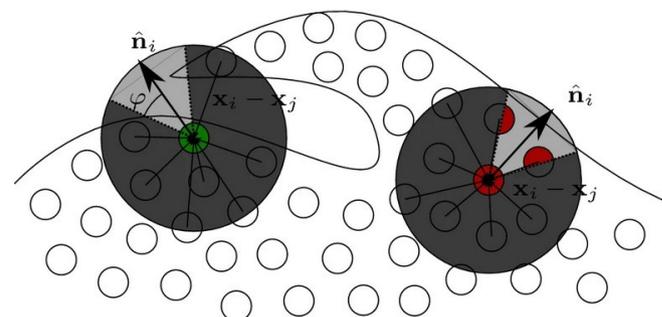**FIGURE 4** Definitions for the surrogate model for the arc heating effect.

FIGURE 5 Coverage-normal, detection of surface particles [11].

$$F_{i,\,T} = \left(\frac{T_V - T_i}{T_V}\right) \quad 0 < F_{i,T} \leq 1 \tag{9}$$

When the material is heated up to the evaporation temperature, no heat is added to the metal.

3.2 | Resistive heating

The heat generation is based on the Joule's heating through resistivity of materials when the current flows through them. Therefore, a tabulated specific electrical resistivity is used. The current density in the wire is calculated by the distribution of the preset welding current on the cross section. The maximum value of the electric current density is assumed for the straight piece of the wire:

$$j = \frac{I}{S_{wire}} \tag{10}$$

After the wire, the current density experiences an inverse proportionate drop.

$$j_{field} = \frac{j}{\left(1 + \frac{(x_{reference\ point} - x_j)}{r_{wire}}\right)} \tag{11}$$

The particle resistance is approximated using sphere geometries with the assumption of current flowing through spherical particles:

$$R_{particle}(T) = \rho_{specific}(T) \cdot \frac{L_{conductor}}{S_{conductor}} \tag{12}$$

The characteristic length of the conductor is approximated by the particle height:

$$L_{conductor} = 2 \cdot r_{particle} \tag{13}$$

The conductor cross-section is approximated by a circular area corresponding to the particle diameter:

$$S_{conductor} = \pi \cdot r_{particle}^2 \tag{14}$$

Thus, the additional energy is distributed in the system by Joule Heating as follows:

$$E_{particle} = j_{field}^2 \cdot R_{particle}(T) \cdot \frac{\Delta t}{m_{particle}} \tag{15}$$

This energy is than added to the volume occupied by the discretization particle raising its temperature.

3.3 | Compensation model for the electromagnetic forces

The Ampère's force law acts as the driving force for droplet detachment, and consequently, for metal transfer. Simply put, this effect is produced by the attraction or repulsion between two wires carrying current, influenced by the self-induced magnetic field generated by the electric current passing through these wires. In the generalized formulation the wires can be represented by abstract streamlines of the electric current. In the specific context of bi-directional wire control mass transfer curved current lines create an even more interesting configuration of acting forces, Figure 3. By vectorially decomposing the local Lorentz forces, which are perpendicular to the current streamlines, forces acting along the main metal transfer direction and in radial direction when assuming an axisymmetric metal transfer bridge, can be created. Adding up the forces in the main metal transfer direction form a resultant force that pulls on the liquid metal and detaches the wire from the weld pool. In the narrowest cross-section the Ampère's force law causes a constriction of the liquid metal bridge by the radial force components. In the presented model, these radial components are not considered to keep the computational effort low and because the effect is small, although for some configurations very important. The approach followed has the goal to first generate a good match with a global process flow with the simplified variant.

In the presented model, the curvature of the streamlines corresponding to the change in cross-section is approximated by the ratio of the radii of the successive layers, Figure 6. These pictures represent the raw format of the results where the field variables are stored within the discretization particles. The resulting Lorentz force F_L is calculated according to equation [18]:

$$F_L = \frac{I^2 \cdot \mu}{4 \cdot \pi} log \frac{r_m}{r_{m+1}} \tag{16}$$

where $I.2$ is an actual current value, μ magnetic constant and r_m the radius of the layer.

The layered force model divides the droplet and the molten metal in the short-circuit phase in 10 layers, Figure 6. The ratios of the cross-section radius of the adjacent layers are determining the magnitude of the force
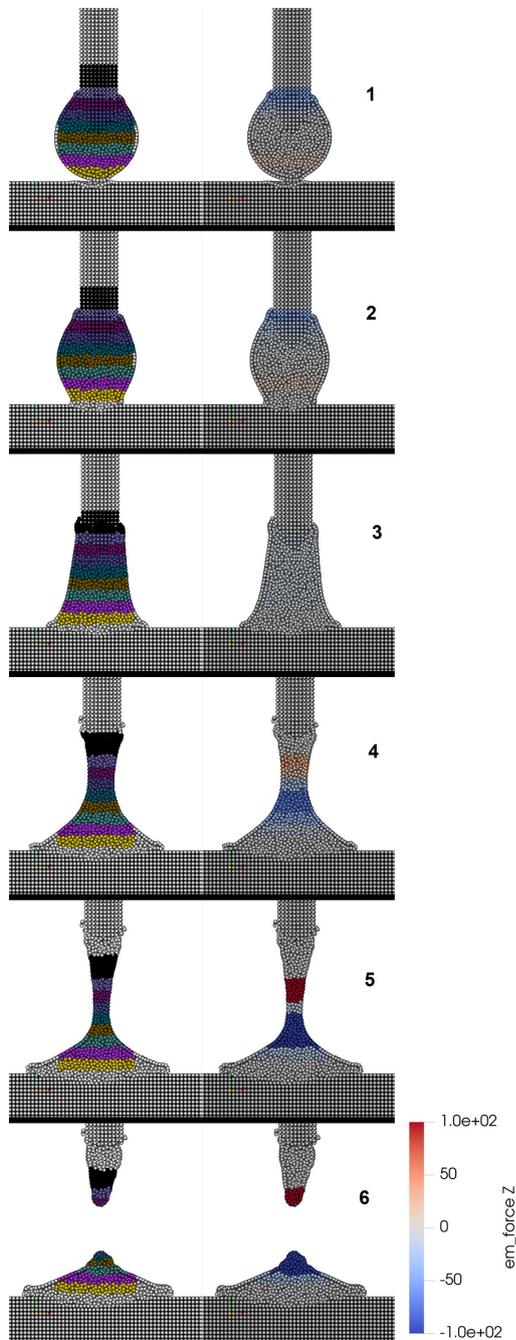
FIGURE 6 Left: layered force model, right: resulting force magnitude.

acting on the fluid, whereby, depending on the ratio, a compressive force that counteracts the detachment can also arise. In the first two images of the sequence the force at the wire tip is acting in the melt pool direction because of the convex shape of the droplet, Figure 6. As the molten metal topology changes to a concave shape, the force acting in the melt pool direction acts under the narrowest cross-section, sequence 4 and 5, Figure 6.

3.4 | The wire movement

The wire is moved according to the specified feed rate v_{wire}:

$$wire_{path} = v_{wire} \cdot \Delta t \cdot \vec{r}_{N,feed} \cdot F_m, \tag{17}$$

where Δt is the time step, $\vec{r}_{N,feed}$ the feed direction and F_m is the multiplier factor for reversing the movement direction of the wire and this factor also contributes to maintaining continuity, Figure 4. The change in wire movement is interpolated due to the multiplier using the following formula:

$$F_m^{t+\Delta t} = F_m^t + \left(F_{m\_t} - F_m^t\right) \cdot 0.2 \tag{18}$$

Thus, the change of the wire movement direction is smoother. The multiplier target factor F_{m_t} is 1.5 for the arc phase and -1 for the short-circuit phase.

The detection of a short-circuit is deployed by a clustering algorithm. Particles in different particle agglomerations get different indices, when they touch each other, a large particle cluster with a unique index for all particles is created, thus the short-circuit is fixed.

After the detection of the short-circuit, the wire is moved up for 3 minutes. After this time, the arc phase starts and the F_{m_t} factor is set to 1.5. The values for the time and the multiplier targets have been chosen after some pretests showing most appropriate accordance to the real process.

4 | RESULTS

The calculations were conducted with a blind weld configuration because the focus was set to investigate the metal transfer. Using typical weld parameters, the process was simulated for four seconds, Table 1. This parameter set represents averaged values and was used for testing models. This is to demonstrate the plausibility of the models used. A weld seam with a realistic temperature distribution was calculated, Figure 7. The calculation was carried out on a 32 cores machine and lasted less than 20 hours.

A more detailed view is given for the droplet detachment, Figure 8. The wire heating is set at a constant height above the workpiece, representing the position of the contact tube. The sequence of the droplet detachment is in good agreement with a real process. A qualitatively comparable temperature distribution in the wire was calculated throughout the detachment sequence.

TABLE 1   Welding parameters.

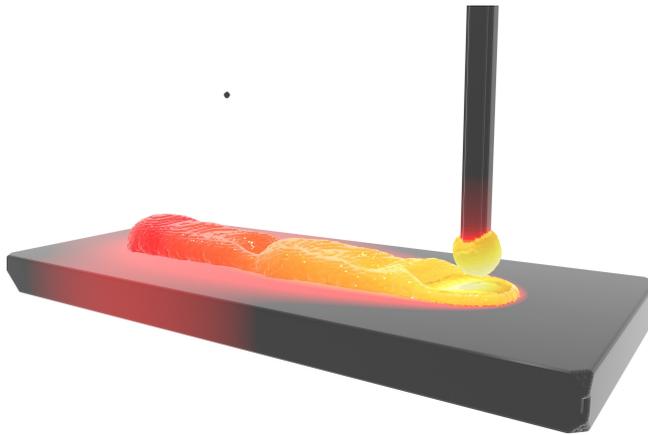| Parameter	Units	
Number of particles		316 143
Process time	s	4
Wire diameter	mm	1
Plate thickness	mm	2
Welding velocity	cm min^{-1}	55
Mean wire feed rate	m min^{-1}	7.5
Welding current	A	200

FIGURE 7   Simulated weld seam of a bi-directional wire control welding process, surface reconstruction.

The comparison is made with the data collected in a study investigating a pulsed gas metal arc welding process [19]. A more precise comparison cannot be offered since the lack of experimental data for the specific welding variant investigated in this study. As expected, in the case of a short-circuit phase, a lower maximal temperature was determined.

5 | DISCUSSION

The presented model describes the transfer of melted metal from the wire to the welding pool in a bi-directional wire control process based on the simplified model for gas metal arc welding in the smoothed particle hydrodynamics formulation. The concept of the model is to separate the subtle processes in the arc region from the heat and mass transfer processes, which exhibit characteristic features for gas metal arc welding. The results presented confirm that the concept works and that the models developed can represent the bi-directional wire control process. The resulting modelling approach is easily transferable to more complex joint topologies, which follows from the intrinsic properties of the
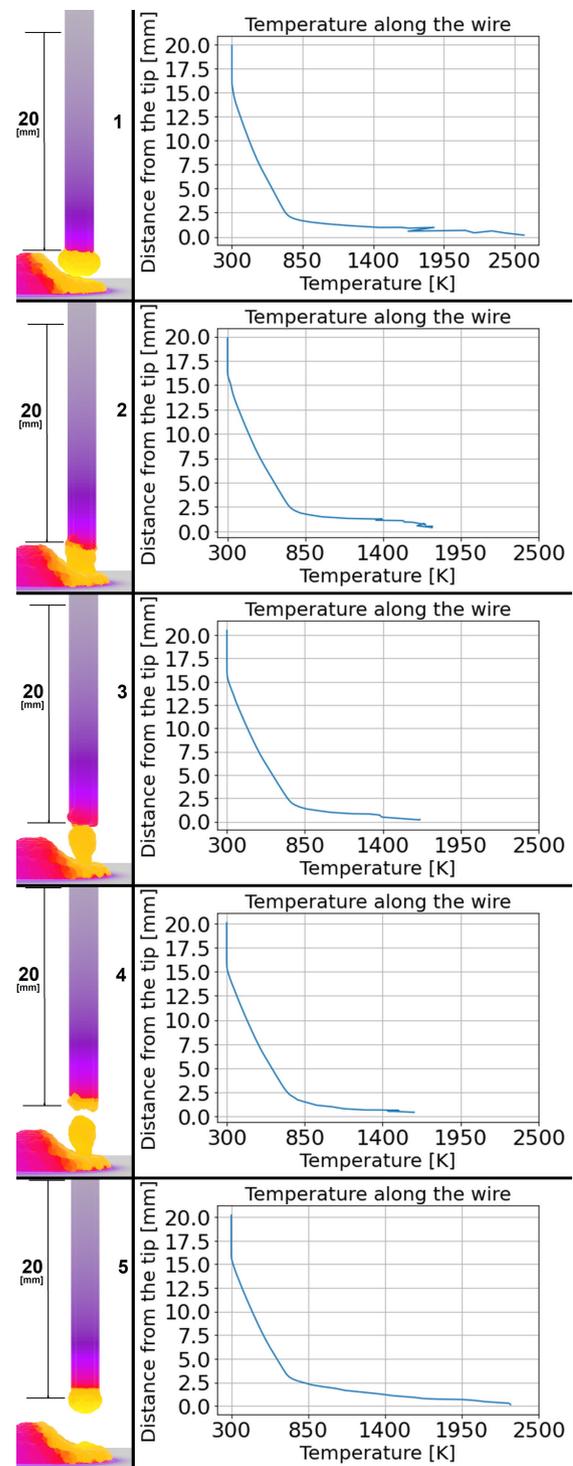

FIGURE 8   Left: simulated characteristic of a bi-directional wire control sequence, right: temperature in the wire centerline.

smoothed particle hydrodynamics method. At the same time, the separation of processes leaves room for a further refined description and realization of the valid gas metal arc welding arc phenomena. This consideration of arc processes, in particular the effects of evaporation on both plasma properties and the distribution of heat and

electric current in the cathode region, may, however, require parallel modelling with intrinsic domains.

Since the bi-directional wire control process is a highly regulated operation the information concerning the control algorithms of the current, voltage and wire fed speed is of great importance for the mapping of quantitatively comparable results. This is a topic for future work.

6 | CONCLUSION

A model for the mass transfer in the bi-directional wire control variant of arc welding is presented. The shown results allow a qualitative evaluation of the used methods. The model is capable to reproduce typical sequences of the arc and short-circuit phase. Despite the simplistic consideration of the physical effects for metal heating as well as arc coupling, the existing model is a very good template for further development.

ORCID
S. Warkentin http://orcid.org/0009-0004-4514-8962
L. Westhofen http://orcid.org/0000-0003-4427-2377
R. Sharma http://orcid.org/0000-0002-6976-4530
U. Reisgen http://orcid.org/0000-0003-4920-2351

REFERENCES
1. P. Kah, R. Suoranta, J. Martikainen, *Int. J. Adv. Manuf. Technol.* **2013**, *67*, 655.
2. S. Selvi, A. Vishvaksenan, E. Rajasekar, *Defence Technology* **2018**, *14*, 28.
3. S. Venukumar, M. Mohan Cheepu, T. Vijayababu, D. Venkateswarlu, *Materials Science Forum* **2019**, *969*, 685.
4. D. Galeazzi, R. H. G. e Silva, I. O. Pigozzo, A. F. d Rosa, A. S. Pereira, C. Marques, *Weld World* **2022**, *66*, 1369.
5. Y. Yuan, R. Li, X. Bi, J. Gu, C. Jiao, *Coatings* **2022**, *12*, 1971.
6. S. Cadiou, M. Courtois, M. Carin, W. Berckmans, P. Le Masson, *Additive Manufacturing* **2020**, *36*, 101541.
7. R. A. Gingold, J. J. Monaghan, *Mon Not R Astron Soc* **1977**, *181*, 375–389.
8. L. B. Lucy, *Astronomical Journal* **1977**, *82*, 1013.
9. D. Koschier, J. Bender, B. Solenthaler, M. Teschner, in: J. Wenzel, P. Enrico (eds) *Eurographics 2019 – Tutorials.*, The Eurographics Association, **2019**.
10. D. J. Price, *Journal of Computational Physics* **2012**, *231*, 759.
11. S. R. Jeske, M. Simon, O. Semenov, J. Kruska, O. Mokrov, R. Sharma, U. Reisgen, J. Bender, *Comp. Part. Mech.* **2023**, *10*, 1.
12. H. Komen, M. Shigeta, M. Tanaka, Y. Abe, T. Fujimoto, M. Nakatani, A. B. Murphy, *Int. J. Heat Mass Transfer* **2021**, *171*, 121062.
13. M. Trautmann, M. Hertel, U. Füssel, *Weld. World* **2018**, *62*, 1365.
14. K. Bobzin, H. Heinemann, K. Jasutyn, S. R. Jeske, J. Bender, S. Warkentin, O. Mokrov, R. Sharma, U. Reisgen, *J Therm Spray Tech* **2023**, *32*, 599.
15. M. Ito, Y. Nishio, S. Izawa, Y. Fukunishi, M. Shigeta, *Trans. JWRI* **2015**, *33*, 34.
16. I. Semenov, I. Krivtsun, U. Reisgen, *J. Phys. D: Appl. Phys.* **2016**, *49*, 105204.
17. O. Mokrov, M. Simon, R. Sharma, U. Reisgen, *J. Phys. D: Appl. Phys.* **2019**, *52*, 364003.
18. V. Pavlyk, O. Mokrov, U. Dilthey, *Heat Source Modelling in GMA-Welding and its Integration in Stress-Strain Analysis*, Mathematical Modelling of Weld Phenomena 8, eds. H. Cerjak et al., TU Graz, **2007**, pp. 801–818.
19. G. Zhang, G. Goett, R. Kozakov, D. Uhrlandt, U. Reisgen, K. Willms, R. Sharma, S. Mann, P. Lozano, *J. Phys. D: Appl. Phys.* **2019**, *52*, 085201.